This is a preprint, the final version is subject to change, of the American Mineralogist (MSA)
Cite as Authors (Year) Title. American Mineralogist, in press.
DOI: https://doi.org/10.2138/am-2019-7095

Diffusion of F and Cl in dry rhyodacitic melt

Yves Feisel[a,*], Jonathan M. Castro[a], Donald B. Dingwell[b,c]

[a] Institute of Geosciences, Johannes Gutenberg-Universität Mainz, 55128 Mainz, Germany

[b] Department für Geo- und Umweltwissenschaften, Ludwig Maximilians Universität München, 80333 München, Germany

[c] Gutenberg Research College, Johannes Gutenberg-Universität Mainz, 55128 Mainz, Germany

*corresponding author: yfeise02@uni-mainz.de

This is a preprint, the final version is subject to change, of the American Mineralogist (MSA)
Cite as Authors (Year) Title. American Mineralogist, in press.
DOI: https://doi.org/10.2138/am-2019-7095

Abstract

Chemical diffusion of F and Cl has been experimentally determined in a rhyodacitic melt obtained from remelting a sample of Hekla pumice (Iceland). Diffusion couple experiments were conducted in a vertical tube furnace over a temperature range of 750 – 950°C and in air for durations of 1 to 35 days. Concentration profiles of F and Cl were obtained for the quenched sample using an electron microprobe.

Fluorine and chlorine exhibit Arrhenian behaviour over the range of temperature investigated here. The pre-exponential factors of F and Cl are $D_0(F) = 4.3 \times 10^{-4}$ and $D_0(Cl) = 1.6 \times 10^{-5}$ m^2/s. Fluorine diffusion coefficients vary in the order of 1×10^{-15} to 1×10^{-13} m^2/s whereas Cl diffusivity is up to 2 orders of magnitude slower. The activation energies for F and Cl diffusivities are equal within error at 223 +/- 31 and 229 +/- 52 kJ/mol, respectively.

The difference in diffusivity between F and Cl is particularly pronounced in the melt of our study, compared to results obtained for other magmatic melt compositions. This means that the potential for diffusive fractionation exists and may occur especially under conditions of magma ascent and bubble growth, as this would favor partitioning of the relatively fast-diffusing halogens into growing bubbles, due to H_2O exsolution. A dependence of diffusivity on atomic radius observed here is enhanced over that observed in more basic, less viscous melts, indicating that diffusive fractionation is more likely to be pronounced in more silicic, more viscous systems. A proper parameterisation and modelling of diffusive fractionation of halogens in actively degassing volcanic systems thus holds the potential of serving as a tool for quantifying the processes responsible for volcanic unrest.

Keywords: halogens (F, Cl); diffusion; silicate melt; diffusion couple; experimental volcanology

This is a preprint, the final version is subject to change, of the American Mineralogist (MSA)
Cite as Authors (Year) Title. American Mineralogist, in press.
DOI: https://doi.org/10.2138/am-2019-7095

1. Introduction

Volatiles are an important constituent of melts and play a significant role in igneous processes. The chemical composition of the volatile phase crucial for the style of volcanic eruptions is dependent on parameters such as solubility, partitioning and diffusion of the different species, which in turn are controlled by compositional parameters (e.g. initial volatile content, magma composition) and ambient conditions (e.g. pressure, temperature). While the dominant components of volcanic volatiles are water (H_2O), carbon dioxide (CO_2), and sulfur-species, halogens (F, Cl, Br, I) can be highly concentrated in silicic melts (e.g. tin and topaz rhyolite, Carroll and Webster, 1994; Webster and Duffield, 1994) and are a significant component of volcanic gases (Symonds et al. 1994; Aiuppa et al. 2009; Webster et al. 2018) venting from active silicic volcanic centers. Halogens affect magma viscosity and diffusivities (e.g. Dingwell et al. 1985; Dingwell and Hess 1998; Baasner et al. 2013) as well as phase equilibria (Manning 1981) and directly influence the stability of hydrous minerals and halogen-bearing phases in igneous rocks (e.g. Micas, Fluorite, Topaz; Webster et al. 2018). Schipper et al. 2017 showed that the degassing of F and Cl into isolated pores of slowly cooling magma can cause silica redistribution and the formation of vapor-phase cristobalite. Halogen degassing is also essential for the formation of ore deposits in active volcanic systems and can have a major impact on Earth's climate and environment including potential destruction of ozone in the stratosphere (Aiuppa et al. 2001, 2009; Bobrowski et al. 2003, 2007; von Glasow et al. 2009; Boichu et al. 2011; Surl et al. 2015; Roberts 2018). The escape of F and Cl from ascending magma has been argued to occur at relatively shallow depths (Spilliaert et al. 2006). Thus, their study in volcanic gas emissions can help identify and characterize pre- or syn-eruptive volcanic degassing and might augment volcano monitoring.

The potential for widely varying diffusivities between the halogens may mean that diffusive fractionation between the halogens may provide further insights into the timing of magma ascent and volatile exsolution (Alletti et al. 2007). Halogens are also increasingly routinely measured in volcanic plumes.

Despite investigations to date, our knowledge of halogen solubility and diffusivity in silicate melts is far from complete. Rhyolitic volcanoes are known to commonly be the most explosive and hazardous and typically comprise melts with the highest F concentrations (e.g. Aiuppa et al., 2009). Yet there, halogen diffusivity data is scant for such systems. Instead, most studies describing volatile behavior in silicate melts have concentrated on H_2O, CO_2 and S. Previous studies on F and Cl diffusion are available for simplified model systems such as albite, jadeite or Na-aluminosilicate (Dingwell and Scarfe, 1984; Dingwell and Scarfe, 1985, only for F), basaltic (Alletti et al. 2007) and phonolitic melts (Balcone-Boissard et al. 2009; Böhm and Schmidt 2013). Only few studies exist on more evolved dacitic to rhyolitic melt compositions (Bai and Koster van Groos 1994; Fortin et al. 2017; Yoshimura 2018) and those have concentrated solely on Cl diffusion. Further, most previous studies have been conducted at higher experimental temperatures than those relevant for natural systems.

While some authors report a pressure dependence of the diffusion coefficients (e.g. 1.0 - 1.5 GPa; Dingwell and Scarfe, 1984; Bai and Koster van Groos, 1994) most recent studies have found only minor pressure effects (e.g. 0.5 - 1.0 GPa, Alletti et al., 2007; Balcone-Boissard et al., 2009). The addition of H_2O is reported to enhance diffusivities up to an order of magnitude (Baker and Balcone-Boissard 2009; Böhm and Schmidt 2013). For a complete compilation of all studies on halogen-diffusion in silicate melts until 2010, see reviews by Baker and Balcone-Boissard (2009) and Zhang et al. (2010) and for a recent comprehensive review about halogens in volcanic systems of mafic to intermediate compositions see Webster et al. (2018).

In this study we apply the diffusion couple technique on remelted, mechanically homogenized glasses synthesized from natural pumice of the Hekla H3 eruption, one of Hekla's most recent Plinian silicic eruptions (2879 BP; 2.2 km^3 DRE; e.g. Sverrisdottir, 2007; Thordarson and Larsen, 2007; Weber and Castro, 2017). We determine the chemical diffusion of F and Cl in melts of rhyodacitic composition over a temperature range relevant for these magmatic systems in order to improve and expand our understanding of volatile transport in magmatic systems. Even though diffusion is not the only mechanism responsible for volatile transport in melts it is one of the fundamental processes necessary to understand and model volcanic degassing.

2. Experimental and analytical technique

The initial sample synthesis was carried out in the laboratories of the Earth Science department of the LMU Munich. Experimental starting glasses were synthesized from natural rhyodacitic pumice of the Hekla H3 eruption (Table 1). The pumice was synthesized in a 1 atm high-T furnace at 1400–1550°C for 2–7 days to produce volatile-depleted glass (Table 1). During the synthesis, the melt was slowly stirred using a platinum-rod attached to a viscometer to improve devolatilization and ensure homogeneity of the whole batch. In addition, the viscosity of the glass was monitored and the synthesis was continued until the viscosity reached a steady state, i.e. the viscosity did not change any more over a time scale of several hours, which we interpreted to reflect the bulk loss of volatiles. After the first synthesis, the batch was split and crushed. One half was doped with halogen-bearing Na-salts (NaF, NaCl, NaBr, NaI) so that each halogen would account for 1 weight percent of the whole batch after doping. Bromine and iodine, even though present in the melt, are the subject of another study in progress. However, it has to be taken into account that all halogen

species are diffusing in our experiments and that this might have an effect on the results. The other, halogen-depleted half of the batch was in turn doped with a certain amount of $NaCO_3$ to account for the sodium enrichment in the halogen-bearing glass. After thorough mixing, each half was then re-homogenized by high-T stirring at the same conditions as in the first synthesizing step for 4–7 days. It is noted that, even though the samples were synthesized at high temperatures for several days, the halogen-depleted sample still contained few 100's of ppms of halogens (Table 1). However, the diffusion of halogens nevertheless occurred under a significant chemical potential gradient between the two diffusion couple halves. The small amount of halogens in the depleted half is therefore not expected to have an effect on the resulting diffusivities. After synthesis, cylinders with a diameter of 4.6 mm were drilled out of the glass within the Pt crucible and cut into small discs with a thickness of ~2 mm using a diamond wire saw. The discs were polished on one side to ensure proper contact between the two diffusion couple halves during the experiment. The final major-element compositions of the two different anhydrous starting glasses are presented in table 1. Sodium enrichment in the experimental glasses compared to the original H3 pumice is attributed to the addition of halogens by Na-halogenides in the enriched and the addition of sodiumcarbonate in the depleted glass.

The capsules for each diffusion couple were constructed from 5 mm Pt tube with a wall-thickness of 0.2 mm. The bottom of the capsule was closed with a Pt lid which was pressed onto and welded to the tube using an arc-welder. Afterwards the bottom of the capsule was tamped down to ensure cylindrical geometry. The halogen-doped glass discs were loaded into the bottom part of the capsules and the halogen-depleted discs on top of them with both discs touching at the polished surfaces (Fig. 1a). Each capsule was closed by welding a second lid to the top of the capsule to ensure closed system conditions (Fig. 1b).

144 The diffusion experiments were conducted in the laboratories of the University of Mainz. For each
145 experiment one diffusion couple was first weighed and then loaded into an alumina tube which is
146 closed on one side. The tube was inserted vertically into a small opening on the top of the vertical
147 tube furnace which was preheated to the target temperature. All experiments were carried out at
148 atmospheric pressure. The capsule was placed upright on the closed bottom of the tube and located
149 in the hot spot of the furnace chamber. The temperature was monitored during the entire run using
150 the internal furnace thermocouple and an additional K-type thermocouple which was in direct
151 contact with the diffusion couple capsule. Temperatures are estimated to be accurate to ± 2°C based
152 on the accuracy of the thermocouple device. The experimental durations ranged from one to 35
153 days depending on the temperature investigated (Table 2). The time needed for the capsule to heat
154 to the target temperature ranged between 3 and 5 minutes. The samples were quenched by sliding
155 the alumina tube out of the furnace and letting it cool in air to room temperature, leaving the
156 assembly in an upright position. Typical cooling times to a temperature of 200°C were in the range
157 of 3 to 4 minutes. After each experiment the samples were weighed again to confirm closed system
158 conditions during the experiment. To investigate a possible pressure effect on halogen diffusion
159 one experiment (HX2b) was conducted at 900°C and 100 MPa in a cold-seal pressure vessel within
160 a horizontal tube furnace. For this experiment Ag-Pd was used as capsule material. Even though
161 heating and quenching times were longer due to the more complex setup, the related error is
162 considered small compared to the long relative experimental durations (see 3.4 for further
163 discussion).
164 After quenching each capsule was embedded in epoxy, cut open parallel to the diffusion direction,
165 and polished for electron microprobe analysis (EMPA). All analyses were performed with an
166 electron microprobe of the type JEOL JXA 8200 in the Department of Geoscience of the University
167 of Mainz. F and Cl concentrations were measured simultaneously along with most major elements.

An acceleration voltage of 15 kV, a beam current of 12 nA and a probe diameter of 5 μm were used for all quantitative analyses. For F and Cl dwell times of 120 s and 30 s were used, respectively. The detection limits for F and Cl were both 60 ppm (1σ). Standards used for calibration are SrF_2 (F), tugtupite (Cl), VG-2 (Ca, Mg), VG-A99 (Fe, Si), MnTi (Mn, Ti) and orthoclase (Al, K). VG-2, VG-A99 and a natural obsidian standard were analyzed repeatedly during each analytical session. The data were corrected with the ZAF method. The profiles were acquired with a step-size of 20 μm on the ends of the profile and smaller step-sizes of 10 and 5 μm for analyses closer to the diffusion interface. This way it was possible to achieve a high spatial resolution of data necessary to resolve slow diffusion but also cover a large range of diffusion widths while keeping analysis time low. Additionally, one qualitative 2D compositional map of F, Cl and some major elements (Si, Al, Na, Ca, Fe, Ti) was acquired for sample HX8 using a pixel-size of 3x3 μm, an acceleration voltage of 15 kV and a beam current of 100 nA. Dwell times were 200 ms for each element.

3. Results

3.1 F and Cl diffusion coefficients

Diffusion coefficients for each experimental temperature were derived from the diffusion profiles acquired by EPMA. In each sample both F and Cl were analyzed. Typical examples of diffusion profiles are presented in Fig. 2. For each sample two profiles with distances ranging from 100 – 700 μm (except only one profile for HX9) were analyzed and processed to confirm homogeneity. Additional backscattered electron images of all samples and a compositional map of sample HX8 (950°C) further confirmed the homogeneity of the major elements and the concentration gradient of F and Cl along the diffusion interface produced by this experimental setup (Fig. 3). The semi-

quantitative compositional map was acquired with a size of 500 x 350 pixels and a spot size of 3 µm. Even though no quantification has been done to the raw data, the map still shows the sharp difference in initial halogen contents of the two diffusion couple halves, in addition to the relative homogeneity of major element composition across the charges. Concentrations of Si, Al, Fe and Ti are very homogeneous in the investigated area. Ca concentration is mostly homogeneous but is enhanced at some points close to the diffusion interface, likely due to the growth of apatite microlites. Na concentration is homogeneous in most parts but is increased in small irregular patches close to the diffusion interface. These Na-rich areas also correspond to low-concentration zones of F and Cl. Profile 2 of HX8 was acquired crossing one of those low-concentration patches. Despite these micro-scale compositional heterogeneities, the compositional map allowed us to select appropriate traverse positions and discard the data points acquired in one of these patches to calculate the diffusion coefficients just from the unaffected data. The compositional map along with backscattered electron images additionally confirmed that no convection occurred in our high-viscosity rhyodacitic diffusion couples. This agrees well with previous studies which demonstrated that even in low-viscosity basaltic melts no convection influenced the experiments (Alletti et al. 2007; Balcone-Boissard et al. 2009). Even though a slight downward bend of the interface was observed in sample HX8 (950°C, Fig. 3a) there is no effect on the resulting diffusion coefficients calculated from linear profiles. A compilation of all analyzed diffusion profiles and the complete compositional map can be found in the supplementary material.

Most concentration profiles show a relatively smooth transition between the enriched and the depleted halves of the sample, which is especially true for the higher temperature runs (e.g. Fig. 2b). Diffusion lengths, i.e. the length over which significant departure from the original concentration occurred, are up to 850 µm for F and 150 µm for Cl in the high-T experiments.

Experiments run at lower temperatures developed only short diffusion profiles (several tens of μm), especially those of Cl. Profiles of Cl concentration in sample HX6 (750°C) were particularly short with only few points falling in the transition zone between enriched and depleted endmembers. Samples HX3 (850°C) and HX4 (800°C) had lower maximum concentrations than all other experiments, supposedly due to our use of a piece of glass that was positioned close to the surface of the stirred sample. Therefore, three additional experiments were performed at the lowest temperatures (750, 800 & 850°C) running for longer experimental duration to improve the diffusion width and thus data quality. However, as diffusivity has previously been shown to be concentration-independent (e.g. Dingwell and Scarfe, 1984; Bai and Koster van Groos, 1994; Baker and Balcone-Boissard, 2009; Zhang et al., 2010), we included the data of HX3 and HX4 in the results.

The diffusion coefficients for each profile and each species were calculated by fitting the concentration data to the concentration-independent equation for constant one-dimensional diffusivity between two semi-infinite media in a cartesian coordinate system (Crank 1975):

$$C(x,t) = \frac{C_{low}+C_{high}}{2} + \frac{C_{low}-C_{high}}{2} * \mathrm{erf}\left(\frac{x-x_0}{2*\sqrt{D*t}}\right) \quad (1)$$

where C(x,t) is the concentration [ppm] at distance x [m] after the experimental time t [s]. C_{low} [ppm] and C_{high} [ppm] are the concentrations of the respective halogen-poor and halogen-enriched starting glasses. Parameter x_0 describes the position of the diffusion interface between the two individual media and D [m^2/s] is the diffusion coefficient. The term *erf* defines the error function. Parameters D, x_0, C_{low} and C_{high} were determined by fitting equation (1) to the respective data. Analyses with totals below 97 wt.% or F and Cl values below 2 times the detection limit (120 ppm, 2σ) were discarded. Fitting was carried out using the non-linear least squares method implemented

239 in a *MatLab*-based computer program. The program is easy to use, offers control over all important
240 parameters and provides the user with information about the goodness of fit (e.g. R^2, plot of
241 residuals etc.) and confidence intervals calculated from the fit. Additionally, the user can fix C_{low}
242 and C_{high} when necessary, e.g. when the profile obtained by EPMA is too short to cover the end-
243 member concentrations of the starting glasses but information about the highest and lowest
244 concentrations is available from another profile analyzed in the same sample. The results obtained
245 by using this program were validated by cross-checking some results with commercially available
246 curve-fitting software (*CurveExpertPro*). Before fitting the data were filtered for outliers. All
247 calculated diffusion coefficients are compiled in table 2 together with the experimental conditions.
248

249 ## 3.2 Temperature dependence of F and Cl diffusion

250

251 Diffusion coefficients of both F and Cl increase with increasing temperature (Fig. 4, Table 2). The
252 calculated diffusion coefficients for F range from 1.6 x 10^{-15} m^2/s (750°C) to 1.3 x 10^{-13} m^2/s
253 (950°C). Those for Cl are up to 2 orders of magnitude smaller and range from 1.7 x 10^{-17} m^2/s
254 (750°C) to 4.5 x 10^{-15} m^2/s (950°C). Diffusion profiles acquired in a single sample may yield
255 slightly different diffusion coefficients (F: <0.2 log units; Cl: <0.5 log units, both except HX7)
256 which partly accounts for the variability in diffusivities, cast in terms of an uncertainty value.
257 However, the results for one sample are in general within the same order of magnitude. Experiment
258 HX2b which was run at elevated pressure of 100 MPa and 900°C yielded diffusion coefficients of
259 F and Cl comparable to those obtained at atmospheric pressure and the same temperature (Table
260 2). We therefore conclude that pressure does not play a significant role in modifying F and Cl
261 diffusion in rhyodacitic melt over a P – T range relevant for volcanic processes. This agrees well

with the findings of other recent studies (Baker and Balcone-Boissard 2009; Zhang et al. 2010; Böhm and Schmidt 2013).

As shown in previous studies F and Cl diffusion in silicate melts follow Arrhenian behavior described by the following equation:

$$D = D_0 * e^{-\frac{E_A}{R*T}} \quad (2)$$

where D is the diffusion coefficient [m^2/s], D_0 is the pre-exponential factor [m^2/s], E_A is the activation energy [J/mol], R is the universal gas constant [8.3145 J/(mol K)] and T is the temperature [K]. In order to determine the constants D_0 and E_A necessary to describe diffusion behavior of the individual species, the diffusion coefficients calculated with equation (1) are plotted in an Arrhenius diagram of log(D) vs. 10000/T [K] (Fig. 4) and the data is fitted to the linear equation:

$$\log(D) = -\frac{E_A}{\ln(10)*R*T} + \log(D_0) \quad (3)$$

E_A correlates with the slope of the line in the Arrhenius diagram and D_0 represents the intercept at 10000/T = 0. From our experiments we calculated pre-exponential factors of $D_0 = 4.3 \times 10^{-4}$ for F and $D_0 = 1.6 \times 10^{-5}$ for Cl. The activation energies of F and Cl are similar (E_A (F) = 223.7 ± 31 kJ/mol; E_A (Cl) = 229.1 ± 52 kJ/mol) as can be seen from the slopes of the trendlines. The uncertainty values of the activation energies represent the 95 % confidence interval calculated during fitting.

3.3 Experimental and analytical uncertainties

The errors given for the diffusion coefficients (Table 2) were calculated during the fitting process and represent the 95 % confidence intervals based on the fitted datapoints only. However, other sources of uncertainty that may have affected the final Arrhenius parameters include: heating and quenching times, spot distance, accuracy of temperature measurements and homogeneity of the glass. After the experiments, few microlites (<1 vol.%) were present in some samples. In particular, some apatite crystals up to 30 μm length crystallized close to the interface mainly in the halogen-depleted sample. However, because we selected analysis traverses so as to avoid these microlites, we did not observe and anomalous F and Cl concentrations. In some samples, small patches of F-depletion and Na-enrichment developed close to the interface (Fig. 3). However, those patches are recognizable from the backscattered images and were either avoided for diffusion profile acquisition or corrected for during data reduction.

Due to the long experimental durations used (minimum 1 day) the short heating and quenching times with a maximum of 5 minutes are considered to have minor effects only. For example, for sample HX8 which had the shortest experimental duration of 87025s (~1 day) the diffusion coefficients for F and Cl would change by only $\pm$ 0.01 x 10^{-13} or 0.02 x 10^{-15} respectively (both <1 %), for experimental durations varying ± 5 minutes. These values are well within the calculated 95 % confidence intervals. For longer experimental durations the error induced by 5 minutes of heating and quenching would be even smaller. For example: an error of 2 hours on the experimental duration of sample HX9 (750°C; ~35 days) would change the resulting diffusion coefficients for F and Cl by less than 1 %. As is shown in the results section, the diffusivities of F and Cl are exceedingly slow, which precludes the development of a significant concentration profile at the relatively short time scales of heating and quenching (max. 10 min total). Even at the highest

temperature investigated, well defined profiles of 500 μm needed one day to develop. Therefore, zero-time experiments have not been carried out. To assess the error introduced by a non-perfect angle between the analyzed profile and the diffusion interface we used the same samples (HX8 and HX9) and calculated the diffusion coefficients for the case that the profile was not perfectly perpendicular to the diffusion interface but tilted by up to 10°. In this case the actual distance between each spot with regard to the diffusion interface would only be ~98 % of the target distance which results in a diffusion coefficient which is smaller by less than 4 % for F and Cl in both samples. The combination of both effects discussed above (5 minutes longer experimental duration and diffusion profile tilted by 10° to the diffusion direction) would result in F and Cl diffusion coefficients both being less than 5 % smaller compared to the apparent value. This is still well within the limits of the 95 % confidence interval calculated from the fit of the concentration profile and is therefore covered by the given error bars. The accuracy of the measured temperature during the experimental run may have an effect on the calculation of the Arrhenian diffusion law. However, the accuracy of the thermocouple device is at least ± 5°C and the thermocouple was in direct contact with the capsule during the whole run. Therefore, we consider the effect of possible temperature deviations to be negligible compared to the relatively large 95 % confidence intervals of the activation energies (Fig. 4).

4. Discussion

4.1 Influence of temperature

Our experiments confirm that diffusion of both F and Cl are strongly positively correlated with temperature and follow Arrhenian behavior (Fig. 4). The temperature dependences of both

elements, represented by their activation energies, are similar and suggest the same diffusion mechanism. However, in the temperature range investigated F diffusion is always faster than Cl diffusion, which is also true for the theoretical case of very low or very high temperatures due to the similar activation energies. The experimental temperatures were chosen according to typical natural magma storage conditions of rhyodacitic systems (e.g. Weber and Castro, 2017). Using the model of Giordano et al. (2008) a glass transition temperature (T_G) of 687°C for the depleted half and 692°C for the enriched half of the diffusion couple was calculated. We consider no significant diffusion to happen below T_G which is supported by the fact that diffusion at 750°C was already so slow it took weeks to develop proper diffusion profiles. Furthermore, at these low temperatures the halves of the diffusion couple did not weld together perfectly over the whole interface, so at lower temperatures the conditions necessary for a diffusion couple would not have been given. However, diffusion at lower temperatures could still take place and could be significant in scenarios of very slow magma ascent rates (e.g. Boudon et al. 2015), or during post-eruptive lava-flow degassing (e.g. Schipper et al. 2015, 2019) rather than explosive eruptions.

4.2 F and Cl diffusion in different melt compositions

Fig. 5 illustrates the results of all published studies on F and Cl diffusion in silicate melts (Watson and Bender 1980; Dingwell and Scarfe 1984, 1985; Bai and Koster van Groos 1994; Alletti et al. 2007; Balcone-Boissard et al. 2009; Böhm and Schmidt 2013; Fortin et al. 2017; Yoshimura 2018). Only the results of anhydrous experiments are shown for better comparability to our study. In general, diffusion coefficients in different silicate melt compositions vary by 3 orders of magnitude for both F and Cl. Melts of basaltic composition yield the highest diffusivities compared to studies on other compositions such as phonolite, dacite or rhyolite. Dingwell and Scarfe (1984, 1985) were

the first to study the diffusion of F in different synthetic silicate melt compositions. Their results for jadeite melt are comparable to those of Alletti et al. (2007) who investigated melts of natural basaltic composition and also studied Cl diffusion. Phonolitic compositions in general yield slower diffusion coefficients for F and Cl with the exception of potassic phonolite from the Laacher See eruption which yields F diffusivities similar to those of basalt (Balcone-Boissard et al. 2009). Böhm and Schmidt (2013) also studied a natural phonolitic composition but at lower temperatures which are potentially more significant to natural systems. They found intermediate diffusivities for F but lower diffusivities for Cl compared to other phonolitic compositions. Watson and Bender (1980) studied tracer diffusion of Cl in a synthetic melt composition and found results similar to basaltic compositions of Alletti et al. (2007).

When our data is extrapolated to the temperature range that has been used by many previous studies (~1200–1450°C), F diffusivity plots close to, yet below that in basalt, jadeite or Na-phonolite, having a very similar activation energy as this determined for dry basalt (Fig. 5a). For Cl, even when the data is extrapolated to high temperatures, diffusivity in our samples is still about one order of magnitude slower than in Na-phonolite and dacite, and even slower compared to other melts (Fig. 5b).

Studies investigating a similar, silicic melt composition are those of Bai and Koster van Groos 1994, Fortin et al. 2017 and Yoshimura 2018. Bai and Koster van Groos (1994) studied Cl diffusion in granitic and haplogranitic melts using different approaches of which the "high-temperature series" is the most similar approach to our study. This set of experiments was run with haplogranitic melt at atmospheric pressure and under dry conditions in a temperature range from 850 – 1400°C. They found a pre-exponential factor of $D_0 = 3.16 \times 10^{-9}$ and a relatively low activation energy of $E_A = 86.2$ kJ/mol. By contrast, our study presents an almost three times larger activation energy and 5 orders of magnitude larger pre-exponential factor resulting in significantly slower

diffusivities than those suggested by Bai and Koster van Groos (1994). This discrepancy is most likely a result of the simplified melt compositions and experimental approaches. Bai and Koster van Groos (1994) equilibrated haplogranitic melt with molten NaCl instead of using a diffusion couple. This way not only diffusion, but also partitioning from the molten NaCl into the melt may influence the results. Yoshimura (2018) used three different experimental setups based on the absorption of Cl to a piece of natural obsidian. The source of Cl was either Cl_2, $Cl_2 + H_2O$ or molten NaCl. At 750 and 950°C and under mostly dry conditions he found $D_{Cl} = 2.0 \times 10^{-17}$ m^2/s and $D_{Cl} = 3.1 \times 10^{-16}$ to 3.3×10^{-15} m^2/s respectively. The lower temperature results (~750–800°C) are based on molten Cl_2 as Cl source and agree well with our findings at the same temperatures. However, at higher temperatures (>800°C) this experimental series yields slower diffusion than our experiments. Instead, the higher value of his 950°C results, based on molten NaCl as Cl source, are similar to our results. It is likely that the results of both of these studies are affected by other mechanisms than pure diffusion, such as solubility and depolymerization of the melt due to Na-infiltration (Yoshimura 2018), of which the latter would result in increased diffusivity. In addition to Na-infiltration, the simplified haplogranitic melt composition used by Bai and Koster van Groos (1994) has likely caused increased diffusivity as a result of the availability of more vacancies within the melt structure compared to a natural melt (see 4.3 for further discussion). The application of their results to natural systems and a direct comparison to our study is therefore difficult. The general results of Fortin et al. 2017 who studied diffusive fractionation of Cl-isotopes in a dacitic melt are comparable to those obtained in our experiments, even though their data were collected at higher temperatures. The enhanced diffusivity in the dacite melt may be explained by the lower content of SiO_2 in addition to the higher amount of network modifying cations (e.g. Fe, Mg) compared to the rhyodacitic composition investigated in this study.

4.3 Effects of melt structure on diffusion

It has been shown in the past that diffusion is highly dependent on the composition of the medium and on its structure (e.g. Jambon and Semet, 1978; Margaritz and Hofmann, 1978; Lowry et al., 1982; Henderson et al., 1985). Typical natural melt compositions comprise a wide range of chemical compositions and vary greatly in their structure which is determined by various parameters such as the amount of SiO_2, network modifying cations, volatiles and the resulting degree of polymerization, defined by parameters such as NBO/T, i.e. the ratio of non-bridging oxygen atoms over tetrahedally coordinated ions (Mysen 1988). The classic interpretation that diffusion in silicate melts depends strongly on the radius of the diffusing element has been shown to be true mainly for noble gases and monovalent cations (Henderson et al. 1985; Lux 1987; Alletti et al. 2007). This strong correlation of diffusivity and atomic radius was interpreted to indicate the movement of these elements through vacancies in the melt structure (Henderson et al. 1985). For divalent and trivalent cations this correlation does not apply, instead the diffusivities of those elements seem to be mostly independent of their respective ionic radius. Rather, Henderson et al. (1985) propose diffusion of divalent and trivalent elements is dominantly controlled by exchange mechanisms that preserve local charge balance and is therefore mainly dependent on the proportion of network modifying cations. Figure 6a illustrates the correlation of atomic radius and diffusivity of the most recent studies on halogen diffusion. The data shown represents diffusivities at 1300°C. As our study and this of Böhm and Schmidt (2013) only provide data up to lower temperatures, diffusion coefficients have been scaled to 1300°C using equation (2). Data of Alletti et al. (2007) follow a behavior similar to di- and trivalent elements for F, Cl and Br in natural basaltic melt, observing almost no correlation between the diffusion coefficient and the atomic radius of the diffusant. Therefore, they interpret the diffusion of halogens in basaltic melt to be dominated by

exchange mechanisms. Our data instead shows consistently slower diffusion of Cl which has a larger radius than F. Other recent experimental data which was mostly obtained from phonolitic compositions also shows a correlation between the diffusivity and the atomic radius, even though very variable and not as strong as observed in our experiments. The correlation of the variable diffusivity between F and Cl and their atomic radius in more evolved melts suggests that the degree of polymerization does have an influence on diffusion and the diffusion mechanism. For a better estimate of the degree of polymerization of the different melts, we calculated NBO/T and the network modifier parameter (SM) for the melts discussed. For NBO/T we followed the method of Mysen (1988) and split FeO_{tot} equally (wt.%) between Fe_2O_3 and FeO (Giordano et al. 2008). SM was calculated after Giordano and Dingwell (2003) as the molar oxide sum of network modifiers: $SM = \sum(Na_2O + K_2O + CaO + MgO + MnO + FeO_{tot}/2)$ [mol.%]. The highest SM value (~32) and the highest NBO/T ratio (0.5) corresponds to the basaltic melt of the study of Alletti et al., (2007) which comprises the fastest diffusion and almost no correlation between the atomic radius and the diffusion coefficient. In contrast, the rhyodacitic melt used in our study has the lowest NBO/T ratio (0.04) and the lowest SM (~12) amongst previous studies and yielded generally slow diffusion with diffusion coefficients of F and Cl differing by up to 2 orders of magnitude. The phonolitic melts (Balcone-Boissard et al. 2009; Böhm and Schmidt 2013) which yield intermediate diffusivities range between NBO/T = 0.08–0.09 with SM ~18–20. However, the K-phonolite series shows only weak correlation between diffusivity and atomic radius similar to the basaltic melt. Figure 6b shows the correlation between parameter SM and the diffusion coefficient of this and other recent studies. From the diagram, it can be seen that diffusivities of F and Cl are expected to be similar at higher SM but deviate significantly with decreasing SM.

In basaltic melts where the proportion of network modifying cations (i.e. SM) is sufficiently high and polymerization is relatively low, diffusion is likely dominated by the charge balancing

453 exchange of ions. As this mechanism mainly depends on the charge of the diffusant, the atomic
454 radius has no significant influence on the diffusion behavior. In more highly polymerized melts
455 with lower SM, ion-exchange is less efficient and diffusion along vacancies in the melt structure
456 becomes more important. However, among elements of the same charge, this mechanism is likely
457 most efficient for those with a small atomic radius, which potentially explains the observed
458 differences in diffusivity between F and Cl in our and other studies. Even though the correlation
459 between D, the proportion of network modifying cations and atomic radius becomes clear with
460 these results there is still the need to investigate the diffusion behavior of other halogens (Br & I)
461 and more intermediate silicate melts to validate and refine this hypothesis.
462 In addition to the obtained diffusion data, the viscosity of the sample material was measured by
463 micropenetration at three different temperatures (690, 720 and 750°C). The viscosities were used
464 to calculate the Eyring diffusivity of oxygen in our melt using the following equation (Glasstone
465 et al. 1941):
466
467 $$D = \frac{k_B * T}{\lambda * \eta} \quad (4)$$
468
469 where k_B is the Boltzmann constant [J/K], T is temperature [K], η is the viscosity [Pas] and λ is the
470 effective jump distance of the diffusant [m], in this case oxygen (2.8 Å, Shimizu and Kushiro,
471 1984). The obtained diffusion coefficients were in turn fitted to the Arrhenius equation in order to
472 extrapolate the Eyring diffusivity to higher temperatures, relevant for our experiments. The
473 calculated diffusivity of oxygen plotted in an Arrhenius diagram has a similar slope (i.e. activation
474 energy) as F and Cl but is located more than 4 orders of magnitude below Cl diffusivity (Fig. 4
475 inset). With this high contrast in diffusivity, the Si-O bonds in the melt appear to behave as if in
476 fixed structural sites relative to the diffusing F- and Cl-ions (Dingwell 1990; Dingwell and Webb

1990), so their diffusion is not affected by self-diffusion of the silicate structure over the relevant time-scales. At higher Eyring mobilities, i.e. lower viscosities, the jump frequency of Si-O bonds would approach the jump frequency of the investigated diffusant and by this the observed diffusivity of F and Cl would likely be increased, as each Si-O jump would allow the diffusing ion to jump to another site as well. Even though the Eyring equation does not predict oxygen diffusivity perfectly (e.g. Liang et al., 1996), it still gives a good approximation of the structurally defined lower limit of transport rates in the melt.

4.4 Potential for diffusive fractionation

The diffusivities presented in section 3 are based upon experiments utilizing dry melt. The main driving force for the growth of bubbles in a natural magma, is however, the exsolution of H_2O and CO_2, neither of which is present in our experimental melt. The following discussion of diffusive fractionation is therefore hypothetical, and based on the assumption that the ratio of diffusivities between F and Cl is equal in dry and wet rhyodacitic melt, which has been shown to be largely the case for other silicic melt compositions by previous studies (e.g. Baker and Balcone-Boissard 2009).

As shown in section 3.1 diffusivities of F and Cl differ by up to 2 orders of magnitude. This variation is likely to produce fractionated volatile compositions during bubble growth, with the faster diffusing F being enriched in the volatile phase compared to the slower diffusing Cl. Recent studies showed that even with only small differences in diffusivity, fractionation can be significant (e.g. Fortin et al. 2017) but is highly dependent on the ratio of the bubble growth rate (R) and the diffusivity (D) ((R/D) Watson 2017), and of course assuming the same vapour-melt partition coefficient (K) for both diffusants. Watson (2017) discussed this relationship on the basis of

different isotopes of the same volatile element, which have the same vapour-melt partition coefficient but small differences in diffusivity and showed that purely diffusive fractionation in bubbles up to 10 mm is most pronounced at R/D values $<10^4$ m^{-1}. However, while the same principles generally apply for other diffusing volatile elements such as F and Cl, the vapour-melt partition coefficient cannot assumed to be identical for both of these elements and thus could greatly influence the exact relative behavior of F and Cl during bubble growth and degassing. In particular, F is known to behave paradoxically in silicate melts, in that it exhibits high solubility in silicic melts (Carroll and Webster 1994) and usually prefers partitioning into melt rather than aqueous fluid (e.g. Lowenstern et al. 2012). However, F degassing during volcanic eruptions is commonly measured, e.g. in volcanic plumes and fumaroles, and preferred partitioning into the vapour phase has been determined experimentally in basaltic compositions (Baker and Alletti 2012). F partitioning may also be influenced by late-stage crystallization of magma, the so-called "second boiling" process. For example, Schipper et al. (2019) showed based on glass inclusion analysis that only 2 wt.% of F and 7 wt.% of Cl were degassed during the 2011-2012 Cordón Caulle eruption's explosive phase, but the bulk of these halogens were later degassed during lava flow emplacement and coincident syn-eruptive laccolith intrusion (Castro et al. 2016). Schipper et al. 2019 postulate that late-stage crystallization of the lava and laccolith played a key role in driving otherwise soluble F out of the melt and into degassing pathways. In summary, the lack of accurate, composition-specific data on the partitioning behavior of F hinders precise modelling of diffusive fractionation of F and Cl during bubble growth. Future experimental efforts could profitably focus on constraining F partitioning in a variety of melt compositions and under a range of different degassing regimes (e.g. open- vs closed-system).

We speculate that diffusive fractionation will be most important when magma ascent rates are slow enough to favor significant transport of F and Cl to growing bubbles, which in turn depends on the

525 characteristic spacing of bubbles within the melt, as determined by bubble number density and size
526 distribution (Gonnermann and Manga 2007). We therefore propose that diffusive halogen
527 fractionation may be most significant during scenarios of slow mass effusion such as lava dome
528 forming eruptions or the slow cooling of lava flows or shallow intrusions (Castro et al. 2016;
529 Schipper et al. 2019).
530

531 # 5. Implications

532

533 Diffusion of F and Cl in dry rhyodacitic melt was characterized experimentally using the diffusion
534 couple technique. Even though the temperature dependence of the two is very similar, there is a
535 large difference in diffusive speeds over the temperature range investigated which suggests that
536 diffusive fractionation with an increasing F/Cl ratio is a possible outcome of magma degassing
537 under conditions of relatively slow ascent and bubble growth, as would be expected during lava
538 dome formation. Diffusion of F and Cl was shown to be generally slower in our rhyodacitic melt
539 compared to basaltic or other simplified silicate melts. We interpret this to be related to the higher
540 degree of polymerization in the rhyodacite melt. This is supported by the fact that the correlation
541 between the atomic radius of the diffusing component and its diffusivity is more pronounced in
542 more silicic, more viscous melts. We propose that concentrations of F and Cl in volcanic gases,
543 when monitored, could help identify volcanic unrest. However, for a comprehensive understanding
544 of diffusive fractionation during degassing, knowledge of halogen fluid/melt partition coefficients
545 in a range of melt compositions are still needed, in addition to other parameters such as bubble
546 nucleation and growth rates under diverse magma ascent scenarios. With these important factors

This is a preprint, the final version is subject to change, of the American Mineralogist (MSA)
Cite as Authors (Year) Title. American Mineralogist, in press.
DOI: https://doi.org/10.2138/am-2019-7095

547 in hand, we anticipate future modeling-based studies on diffusive fractionation processes at
548 volcanoes (e.g. Watson 2017).

Acknowledgements

This research is part of the Ph.D. thesis of Y. Feisel and is supported a fellowship of the Gutenberg Research College of the Johannes Gutenberg-University of Mainz to D.B. Dingwell. Additional support was provided by the VAMOS research center of the Johannes Gutenberg-University. We thank B. Scheu, U. Küppers, and K.-U. Hess for their assistance during sample preparation and N. Groschopf and S. Buhre for their assistance with electron microprobe analyses. B. Watson, H. Balcone-Boissard and one anonymous reviewer are thanked for their insightful comments which helped to improve this paper.

References

Aiuppa, A., Bonfanti, P., Brusca, L., D'Alessandro, W., Federico, C., and Parello, F. (2001) Evaluation of the environmental impact of volcanic emissions from the chemistry of rainwater: Mount Etna area (Sicily). Applied Geochemistry, 16, 985–1000.

Aiuppa, A., Baker, D.R., and Webster, J.D. (2009) Halogens in volcanic systems. Chemical Geology, 263, 1–18.

Alletti, M., Baker, D.R., and Freda, C. (2007) Halogen diffusion in a basaltic melt. Geochimica et Cosmochimica Acta, 71, 3570–3580.

Baasner, A., Schmidt, B.C., and Webb, S.L. (2013) Compositional dependence of the rheology of halogen (F, Cl) bearing aluminosilicate melts. Chemical Geology, 346, 172–183.

Bai, T.B., and Koster van Groos, A.F. (1994) Diffusion of chlorine in granitic melts. Geochimica et Cosmochimica Acta, 58, 113–123.

Baker, D.R., and Alletti, M. (2012) Fluid saturation and volatile partitioning between melts and hydrous fluids in crustal magmatic systems: The contribution of experimental measurements and solubility models. Earth-Science Reviews, 114, 298–324.

Baker, D.R., and Balcone-Boissard, H. (2009) Halogen diffusion in magmatic systems: Our current state of knowledge. Chemical Geology, 263, 82–88.

Balcone-Boissard, H., Baker, D.R., Villemant, B., and Boudon, G. (2009) F and Cl diffusion in phonolitic melts: Influence of the Na/K ratio. Chemical Geology, 263, 89–98.

578 Bobrowski, N., Hönninger, G., Galle, B., and Platt, U. (2003) Detection of bromine monoxide in
579 a volcanic plume. Nature, 423, 273–276.

580 Bobrowski, N., von Glasow, R., Aiuppa, A., Inguaggiato, S., Louban, I., Ibrahim, O.W., and
581 Platt, U. (2007) Reactive halogen chemistry in volcanic plumes. Journal of Geophysical
582 Research Atmospheres, 112.

583 Böhm, A., and Schmidt, B.C. (2013) Fluorine and chlorine diffusion in phonolitic melt. Chemical
584 Geology, 346, 162–171.

585 Boichu, M., Oppenheimer, C., Roberts, T.J., Tsanev, V., and Kyle, P.R. (2011) On bromine,
586 nitrogen oxides and ozone depletion in the tropospheric plume of Erebus volcano
587 (Antarctica). Atmospheric Environment, 45, 3856–3866.

588 Boudon, G., Balcone-Boissard, H., Villemant, B., and Morgan, D.J. (2015) What factors control
589 superficial lava dome explosivity? Scientific Reports, 5.

590 Carroll, M.R., and Webster, J.D. (1994) Solubilities of sulfur, noble gases, nitrogen, chlorine, and
591 fluorine in magmas. In M.R. Carroll and J.R. Holloway, Eds., Volatiles in Magmas Vol. 30,
592 pp. 231–279. Rev. Mineral.

593 Castro, J.M., Cordonnier, B., Schipper, C.I., Tuffen, H., Baumann, T.S., and Feisel, Y. (2016)
594 Rapid laccolith intrusion driven by explosive volcanic eruption. Nature Communications, 7.

595 Crank, J. (1975) The Mathematics of Diffusion. Clarendon-Oxford, London.

596 Dingwell, D.B. (1990) Effects of structural relaxation on cationic tracer diffusion in silicate
597 melts. Chemical Geology, 82, 209–216.

598 Dingwell, D.B., and Hess, K.U. (1998) Melt viscosities in the system Na-Fe-Si-O-F-Cl;
599 contrasting effects of F and Cl in alkaline melts. American Mineralogist, 83, 1016–1021.

600 Dingwell, D.B., and Scarfe, C.M. (1984) Chemical diffusion of fluorine in jadeite melt at high
601 pressure. Geochimica et Cosmochimica Acta, 48, 2517–2525.

602 Dingwell, D.B., and Scarfe, C.M. (1985) Chemical diffusion of fluorine in melts in the system
603 Na20-Al203-SiO2. Earth and Planetary Science Letters, 73, 377–384.

604 Dingwell, D.B., and Webb, S.L. (1990) Relaxation in silicate melts. European Journal of
605 Mineralogy, 2, 427–449.

606 Dingwell, D.B., Scarfe, C.M., and Cronin, D.J. (1985) The effect of fluorine on viscosities in the
607 system sodium monoxide-aluminum oxide-silicon dioxide: implications for phonolites,
608 trachytes and rhyolites. American Mineralogist, 70, 80–87.

609 Fortin, M.A., Watson, E.B., and Stern, R. (2017) The isotope mass effect on chlorine diffusion in
610 dacite melt, with implications for fractionation during bubble growth. Earth and Planetary
611 Science Letters, 480, 15–24.

612 Giordano, D., and Dingwell, D.B. (2003) Non-Arrhenian multicomponent melt viscosity: A
613 model. Earth and Planetary Science Letters, 208, 337–349.

614 Giordano, D., Russell, J.K., and Dingwell, D.B. (2008) Viscosity of magmatic liquids: A model.
615 Earth and Planetary Science Letters, 271, 123–134.

616 Glasstone, S., Laidler, K.J., and Eyring, H. (1941) The Theory of Rate Processes. McGraw-Hill,
617 New York.

618 Gonnermann, H.M., and Manga, M. (2007) The Fluid Mechanics Inside a Volcano. Annual
619 Review of Fluid Mechanics, 39, 321–356.

620 Henderson, P., Nolan, J., Cunningham, G.C., and Lowry, R.K. (1985) Structural controls and
621 mechanisms of diffusion in natural silicate melts. Contributions to Mineralogy and
622 Petrology, 89, 263–272.

623 Jambon, A., and Semet, M.P. (1978) Lithium diffusion in silicate glasses of Albite, Orthoclase,
624 and Obsidian composition: an ion-microprobe determination. Earth and Planetary Science
625 Letters, 37, 445–450.

626 Liang, Y., Richter, F.M., Davis, A.M., and Bruce Watson, E. (1996) Diffusion in silicate melts: I.
627 Self diffusion in CaO□ Al< sub> 2</sub> 0< sub> 3</sub>□ SiO< sub> 2</sub> at 1500°
628 C and 1 GPa. Geochimica et Cosmochimica Acta, 60, 4353–4367.

629 Lowenstern, J.B., Bleick, H., Vazquez, J.A., Castro, J.M., and Larson, P.B. (2012) Degassing of
630 Cl, F, Li, and Be during extrusion and crystallization of the rhyolite dome at Volcán
631 Chaitén, Chile during 2008 and 2009. Bulletin of Volcanology, 74, 2303–2319.

632 Lowry, R.K., Hender, P., and Nolan, J. (1982) Tracer Diffusion of Some Alkali, Alkaline-Earth
633 and Transition Element Ions in a Basaltic and an Andesitic Melt, and the Implications
634 Concerning Melt Structure. Contributions to Mineralogy and Petrology, 80, 254–261.

635 Lux, G. (1987) The behavior of noble gases in silicate liquids: Solution, diffusion, bubbles and
636 surface effects, with applications to natural samples. Geochimica et Cosmochimica Acta, 51,
637 1549–1560.

638 Manning, D.A.C. (1981) The Effect of Fluorine on Liquidus Phase relationships in the System

639 Qz--Ab--Or with Excess Water at 1 kb. Contributions to Mineralogy and Petrology, 76,
640 206–215.

641 Margaritz, M., and Hofmann, A.W. (1978) Diffusion of Sr, Ba and Na in obsidian. Geochimica et
642 Cosmochimica Acta, 42, 595–605.

643 Mysen, B.O. (1988) Structure and Properties of Silicate Melts. Elsevier, Amsterdam.

644 Roberts, T. (2018) Ozone Depletion in Tropospheric Volcanic Plumes: From Halogen-Poor to
645 Halogen-Rich Emissions. Geosciences, 8, 68.

646 Schipper, C.I., Castro, J.M., Tuffen, H., Wadsworth, F.B., Chappell, D., Pantoja, A.E., Simpson,
647 M.P., and Le Ru, E.C. (2015) Cristobalite in the 2011–2012 Cordón Caulle eruption (Chile).
648 Bulletin of Volcanology, 77.

649 Schipper, C.I., Castro, J., Kennedy, B., Christenson, B., Aiuppa, A., Alloway, B., Forte, P.,
650 Seropian, G., and Tuffen, H. (2019) Halogen (Cl, F) release during explosive, effusive, and
651 intrusive phases of the 2011 rhyolitic eruption at Cordón Caulle volcano (Chile). Volcanica,
652 2, 73–90.

653 Schipper, I.C., Mandon, C., Maksimenko, A., Castro, J.M., Conway, C.E., Hauer, P., Kirilova,
654 M., and Kilgour, G. (2017) Vapor-phase cristobalite as a durable indicator of magmatic pore
655 structure and halogen degassing: an example from White Island volcano (New Zealand).
656 Bulletin of Volcanology, 79, 74.

657 Shimizu, N., and Kushiro, I. (1984) Diffusivity of oxygen in jadeite and diopside melts at high
658 pressures. Geochimica et Cosmochimica Acta, 48, 1295–1303.

659 Spilliaert, N., Métrich, N., and Allard, P. (2006) S-Cl-F degassing pattern of water-rich alkali

basalt: Modelling and relationship with eruption styles on Mount Etna volcano. Earth and Planetary Science Letters, 248, 772–786.

Surl, L., Donohoue, D., Aiuppa, A., Bobrowski, N., and Von Glasow, R. (2015) Quantification of the depletion of ozone in the plume of Mount Etna. Atmospheric Chemistry and Physics, 15, 2613–2628.

Sverrisdottir, G. (2007) Hybrid magma generation preceding Plinian silicic eruptions at Hekla, Iceland: Evidence from mineralogy and chemistry of two zoned deposits. Geological Magazine, 144, 643–659.

Symonds, R.B., Rose, W.I., Bluth, G.J.S., and Gerlach, T.M. (1994) Volcanic-gas studies: methods, results, and applications. In M.R. Carroll and J.R. Holloway, Eds., Volatiles in Magmas Vol. 30, pp. 1–66. Rev. Mineral.

Thordarson, T., and Larsen, G. (2007) Volcanism in Iceland in historical time: Volcano types, eruption styles and eruptive history. Journal of Geodynamics, 43, 118–152.

von Glasow, R., Bobrowski, N., and Kern, C. (2009) The effects of volcanic eruptions on atmospheric chemistry. Chemical Geology, 263, 131–142.

Watson, E.B. (2017) Diffusive fractionation of volatiles and their isotopes during bubble growth in magmas. Contributions to Mineralogy and Petrology, 172.

Watson, E.B., and Bender, J.F. (1980) Diffusion of cesium, samarium, strontium, and chlorine in molten silicate at high temperatures and pressures. Geological Society of America, Abstracts with Programs, 12, 545.

Weber, G., and Castro, J.M. (2017) Phase petrology reveals shallow magma storage prior to large

681 explosive silicic eruptions at Hekla volcano, Iceland. Earth and Planetary Science Letters,
682 466, 168–180.

683 Webster, J.D., and Duffield, W.A. (1994) Extreme Halogen Abundances in Tin-Rich Magma of
684 the Taylor Creek Rhyolite, New Mexico. Economic Geology, 89, 849–850.

685 Webster, J.D., Baker, D.R., and Aiuppa, A. (2018) Halogens in Mafic and Intermediate-Silica
686 Content Magmas. In D.E. Harlov and L.Y. Aranovich, Eds., The Role of Halogens in
687 Terrestrial and Extraterrestrial Geochemical Processes pp. 307–430. Springer-Verlag.

688 Yoshimura, S. (2018) Chlorine diffusion in rhyolite under low-H 2 O conditions. Chemical
689 Geology, 483, 619–630.

690 Zhang, Y., Ni, H., and Chen, Y. (2010) Diffusion Data in Silicate Melts. In Y. Zhang and D.J.
691 Cherniak, Eds., Reviews in Mineralogy and Geochemistry Vol. 72, pp. 311–408. Rev.
692 Mineral.

693

This is a preprint, the final version is subject to change, of the American Mineralogist (MSA)
Cite as Authors (Year) Title. American Mineralogist, in press.
DOI: https://doi.org/10.2138/am-2019-7095

Tables and table captions

Table 1: *Chemical composition of Hekla H3 pumice and the resulting synthesized glasses. Synthesized compositions include corrections for Na-loss. Major elements are normalized to 100 wt.%.*

	H3 pumice[a]	enriched glass	1 SD	depleted glass	1 SD
wt.%	whole rock	*n* = 15		*n* = 14	
SiO_2	69.93	68.47	0.35	68.26	0.31
TiO_2	0.34	0.46	0.02	0.46	0.02
Al_2O_3	14.72	14.70	0.12	14.57	0.08
FeO	4.83	4.60	0.29	4.76	0.06
MgO	0.13	0.46	0.02	0.44	0.02
MnO	0.14	0.13	0.02	0.15	0.02
CaO	2.66	2.85	0.07	2.82	0.05
Na_2O	4.85	6.24	0.12	6.35	0.07
K_2O	2.33	2.10	0.03	2.20	0.03
P_2O_5	0.05	-	-	-	-
F	[a]	0.53	0.02	0.04	0.03
Cl	[a]	0.26	0.01	0.02	0.02
Total	99.1	101.35	0.33	100.07	0.43

[a] data from Weber and Castro (2017) obtained by XRF. Significant F (1800 ppm) and Cl (500 ppm) concentrations are reported for matrix glass analyses (EPMA) of the H3 pumice.

Table 2: *Conditions and results of all experiments.*

sample	**T [°C]**	**time [s]**	profile #	**D_F**	±[a]	C_{max}	C_{min}	**D_{Cl}**	±[a]	C_{max}	C_{min}
HX6	750	851880	1	1.6E-15	3.8E-16	5428	944	5.2E-17	7.8E-17	2647	292
			2	2.1E-15	5.7E-15	5473	988	7.5E-17	4.0E-17	2710	320
HX9	750	3023535	1	1.6E-15	4.3E-16	5657	996	1.7E-17	8.4E-18	2881	353
HX4	800	359334	1	2.6E-15	9.1E-16	3355	548	4.6E-17	3.5E-17	1083	189
			2	3.2E-15	1.3E-15	3409	498	8.6E-17	1.3E-16	1057	188
HX7	800	587235	1	6.6E-15	1.6E-16	5549	758	4.9E-17	1.4E-17	2732	257
			2	1.1E-14	1.9E-15	5580	671	1.6E-16	4.2E-17	2714	291
HX3	850	171502	1	1.6E-14	5.0E-15	3829	1045	3.9E-16	2.0E-16	1534	326
			2	1.9E-14	5.9E-15	3928	1014	4.5E-16	2.4E-16	1471	319
HX10	850	266855	1	1.9E-14	4.4E-15	5624	947	3.9E-16	1.2E-16	2740	318
			2	2.0E-14	5.1E-15	5482	970	7.4E-16	4.0E-16	2733	315
HX5	900	154560	1[b]	4.7E-14	6.7E-15	5186	501	1.0E-15	2.0E-16	2762	222
			2	4.6E-14	8.9E-15	5186	501	8.7E-16	1.9E-16	2758	196
HX8	950	87025	1	1.3E-13	2.5E-14	5491	917	4.5E-15	1.1E-15	2721	302
			2	1.1E-13	1.4E-14	5304	993	1.5E-15	6.7E-16	2715	294
HX2b[c]	900	83400	1	4.7E-14	9.3E-15	5507	832	1.4E-15	4.8E-16	2726	310
			2	3.4E-14	9.2E-15	5320	859	1.3E-15	4.0E-16	2747	311

[a] 95% confidence interval calculated from the fit
[b] C_{max} and C_{min} of F fixed from profile 2
[c] experiment run at 100 MPa

This is a preprint, the final version is subject to change, of the American Mineralogist (MSA)
Cite as Authors (Year) Title. American Mineralogist, in press.
DOI: https://doi.org/10.2138/am-2019-7095

Figure captions

Fig. 1: Capsule geometry used for diffusion couple experiments. a) Schematic section through an experimental capsule. b) Finished capsule before the experiment.

Fig. 2: Representative concentration – distance diagrams of F and Cl obtained by electron microprobe analysis. Also shown are the corresponding fits of equation 3.1 and the respective diffusion coefficients as determined by fitting. a) sample HX9 (750°C / ~35 days) b) sample HX10 profile # 1 (850°C / ~3 days)

Fig. 3: Results of point- and map-analysis of sample HX8 (950°C). a) Backscattered electron image showing the slightly bent diffusion interface and irregular lower density patches (darker). Yellow lines show the position of two profiles acquired with point-analysis. b) Diffusion concentrations determined for F and Cl along the left profile in a), from A to B. c) Compositional maps of F, Cl, Na and Si. Maps of F and Cl show a clear concentration gradient parallel to the diffusion interface. Note the high homogeneity of Si and Na apart from irregular patches of Na enrichment. Please see text for further discussion.

Fig. 4: Diffusion coefficients for F and Cl determined in this study plotted on an Arrhenius diagram. Solid symbols represent experiments at 1 atm while open gray symbols represent pressurized conditions (100 MPa). Results from the 100 MPa series have not been used for fitting. The inlet shows the position of the Arrhenius laws of F and Cl relative to the calculated self-diffusion of oxygen. See 4.3 for further explanation. Error bars correspond to the 95 % confidence-

interval calculated from fitting of the diffusion coefficients. Errors in x-direction are within the symbol-size.

Fig. 5: Overview of Arrhenian diffusion for different melt compositions determined in this and other studies. a) Fluorine b) Chlorine. Results of experiments using dry compositions are shown only. Bold lines represent data obtained in this study and dashed line shows the same data extrapolated to higher temperatures. Note the different y-axis scaling between the diagrams.

Fig. 6: Diagrams showing the correlation of diffusivity with the atomic radius and the sum of the network modifying cations of this and other recent studies. a) Atomic radius vs. D. D of basalt and Na-phonolite show only weak correlation with the atomic radius, while diffusion in rhyodacite is strongly correlated. Lines marked with "*" are calculated from equation (2). b) Diffusivity of F and Cl as a function of the proportion of network modifying cations in the host melt, represented by the parameter SM (= $\sum Na_2O + K_2O + CaO + MgO + MnO + FeO_{tot}/2$ [mol.%]). Dashed lines indicate a simplified exponential fit of the form $y = ae^{bx}$ for each set of datapoints. As they both represent the same SM value, Na- and K-phonolite together have been accounted for as one datapoint with averaged D. All diffusivities presented are for anhydrous conditions at 1250°C. See text for further discussion.

This is a preprint, the final version is subject to change, of the American Mineralogist (MSA)
Cite as Authors (Year) Title. American Mineralogist, in press.
DOI: https://doi.org/10.2138/am-2019-7095

Fig. 1

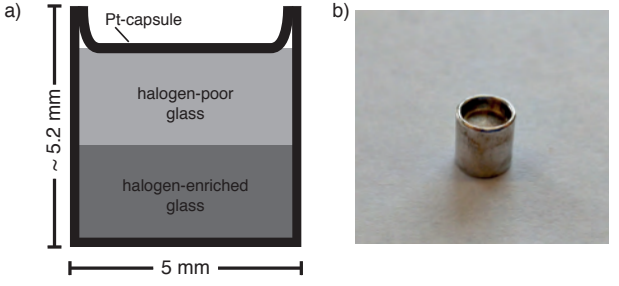

This is a preprint, the final version is subject to change, of the American Mineralogist (MSA)
Cite as Authors (Year) Title. American Mineralogist, in press.
DOI: https://doi.org/10.2138/am-2019-7095

Fig. 2

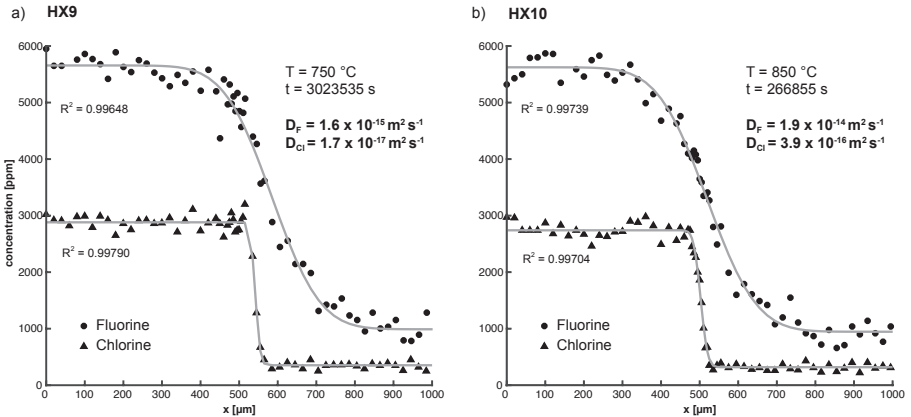

This is a preprint, the final version is subject to change, of the American Mineralogist (MSA)
Cite as Authors (Year) Title. American Mineralogist, in press.
DOI: https://doi.org/10.2138/am-2019-7095

Fig. 3

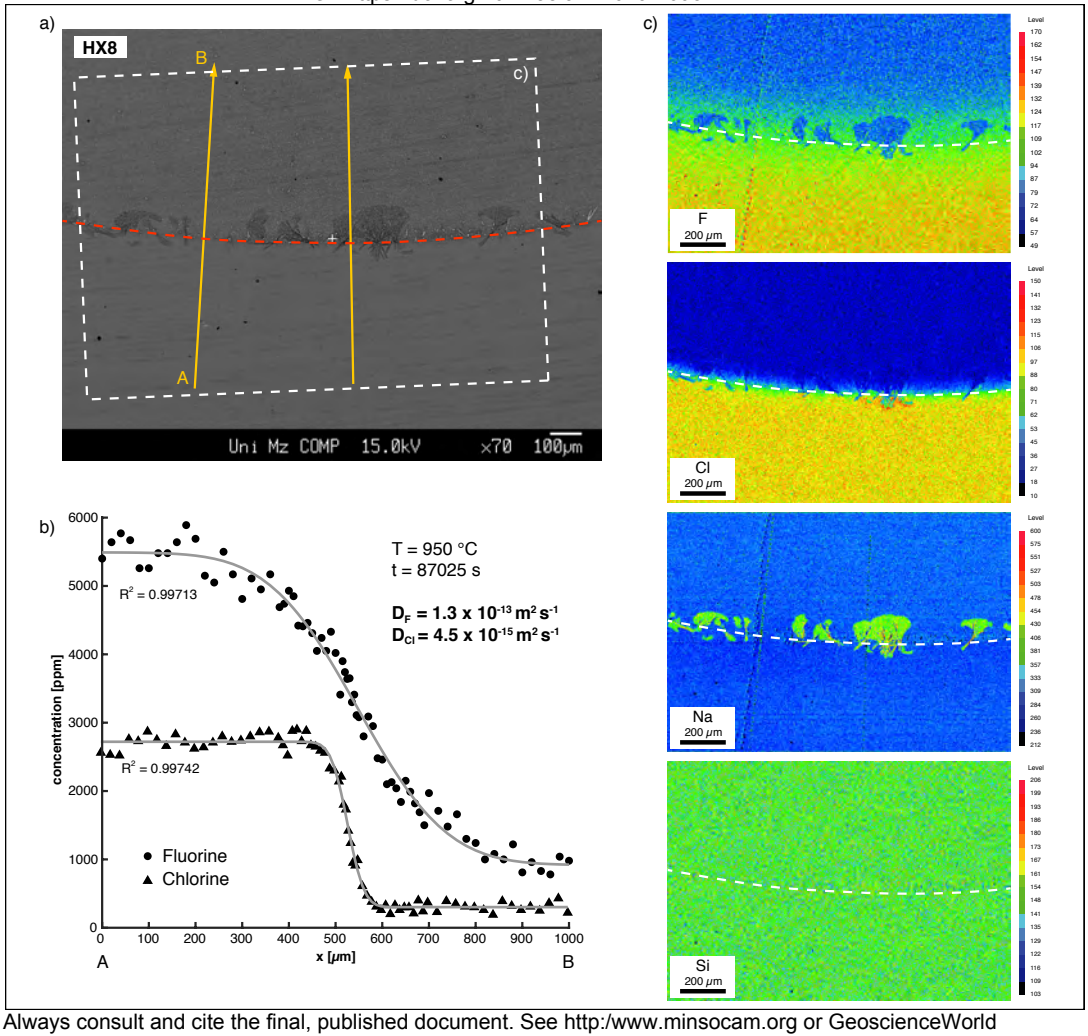

This is a preprint, the final version is subject to change, of the American Mineralogist (MSA)
Cite as Authors (Year) Title. American Mineralogist, in press.
DOI: https://doi.org/10.2138/am-2019-7095

Fig. 4

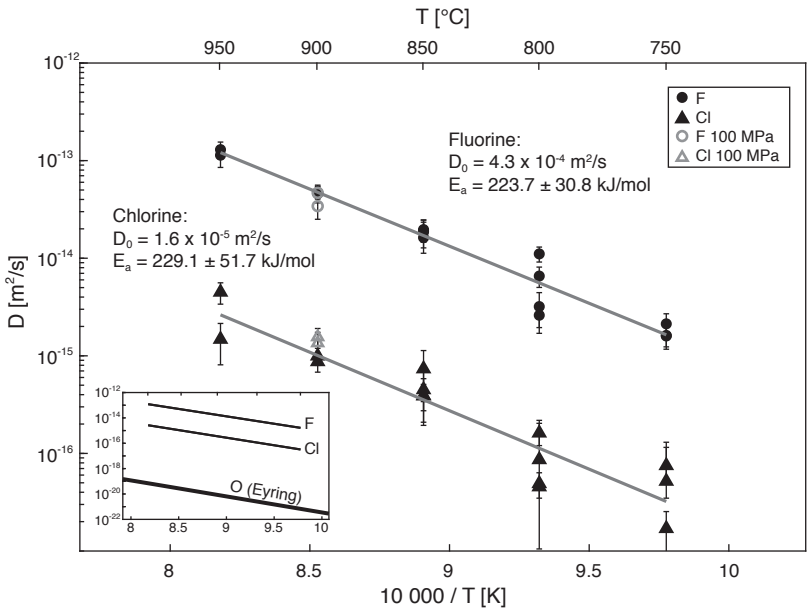

This is a preprint, the final version is subject to change, of the American Mineralogist (MSA)
Cite as Authors (Year) Title. American Mineralogist, in press.
DOI: https://doi.org/10.2138/am-2019-7095

Fig. 5

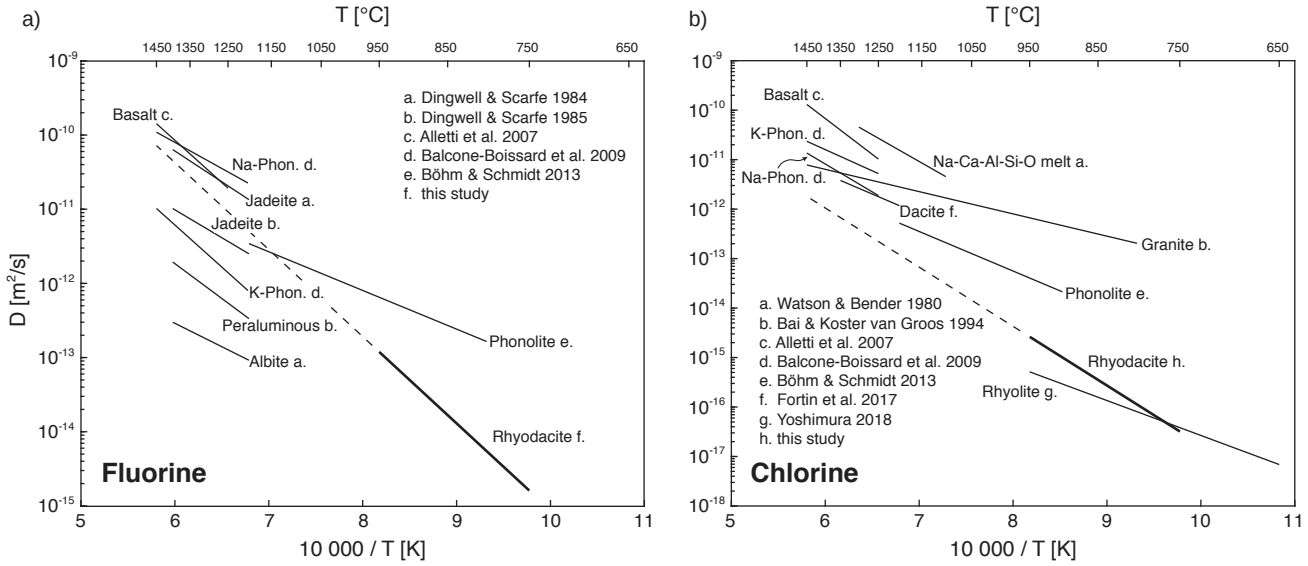

This is a preprint, the final version is subject to change, of the American Mineralogist (MSA)
Cite as Authors (Year) Title. American Mineralogist, in press.
DOI: https://doi.org/10.2138/am-2019-7095

Fig. 6